Electronic Supplementary Material (ESI) for Lab on a Chip

Supplemental information for:

Microstructure-induced helical vortices allow single-stream and long-term inertial focusing

by

*Aram J. Chung, Dianne Pulido, Justin C. Oka, Hamed Amini, Mahdokht Masaeli and Dino Di Carlo**

Normalized transport

The normalized transport is defined as $\sigma \equiv V_{max} / U_{avg}$ where V_{max} is the maximum net lateral velocity in YZ-plane and U_{avg} is the average downstream velocity.[1]

Net lateral velocity

Net lateral velocity is introduced as reported by Amini *et al.*[1] The net lateral velocity field is defined as $\boldsymbol{V}(y, z) = (V_y, V_z)$ where,

$$V_y(y,z) = \frac{\int_{x_1}^{x_2} \left\{ U_y(x,y,z)_{fluid} \right\} \cdot dx}{\Delta x} \quad \text{and} \quad V_z(y,z) = \frac{\int_{x_1}^{x_2} \left\{ U_z(x,y,z)_{fluid} \right\} \cdot dx}{\Delta x}.$$

Supplemental Figures

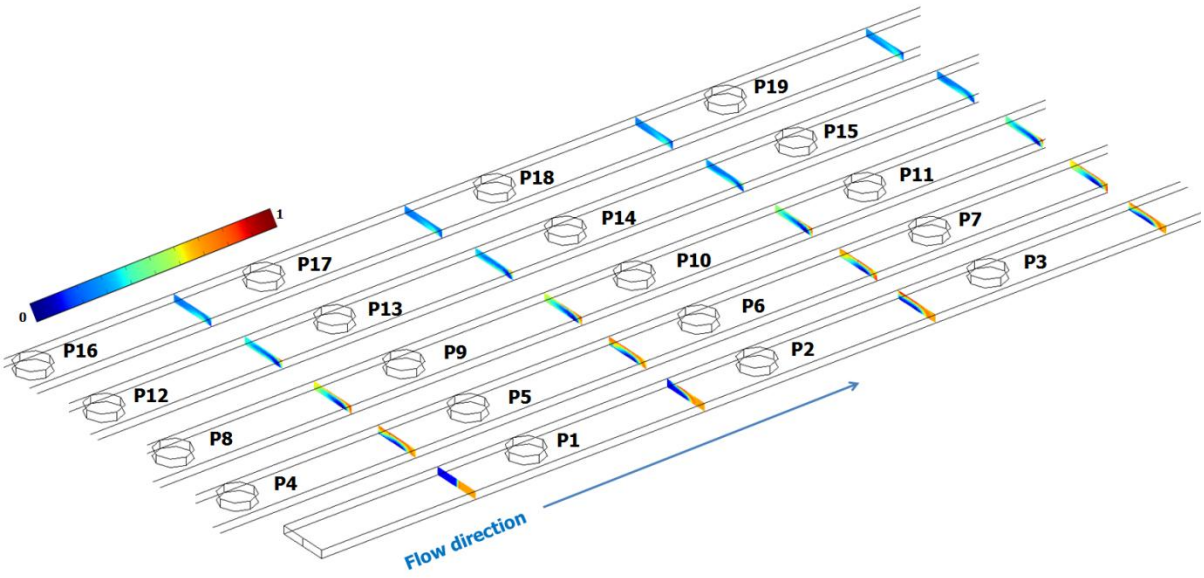

Figure S1. FEM numerical simulations. Helical flow motion induced by single and multiple pillars were numerically investigated using COMSOL Multiphysics (Comsol, Inc., MA, USA) as previously described.[2] In short, the three-dimensional flow field solution (at Re = 66.7) was obtained using the full three-dimensional incompressible Navier-Stokes equations and the calculated velocity field was then used to solve the convection-diffusion equation for species transport. In all cases, only the top-half of the domain was calculated due to the symmetry of the system.

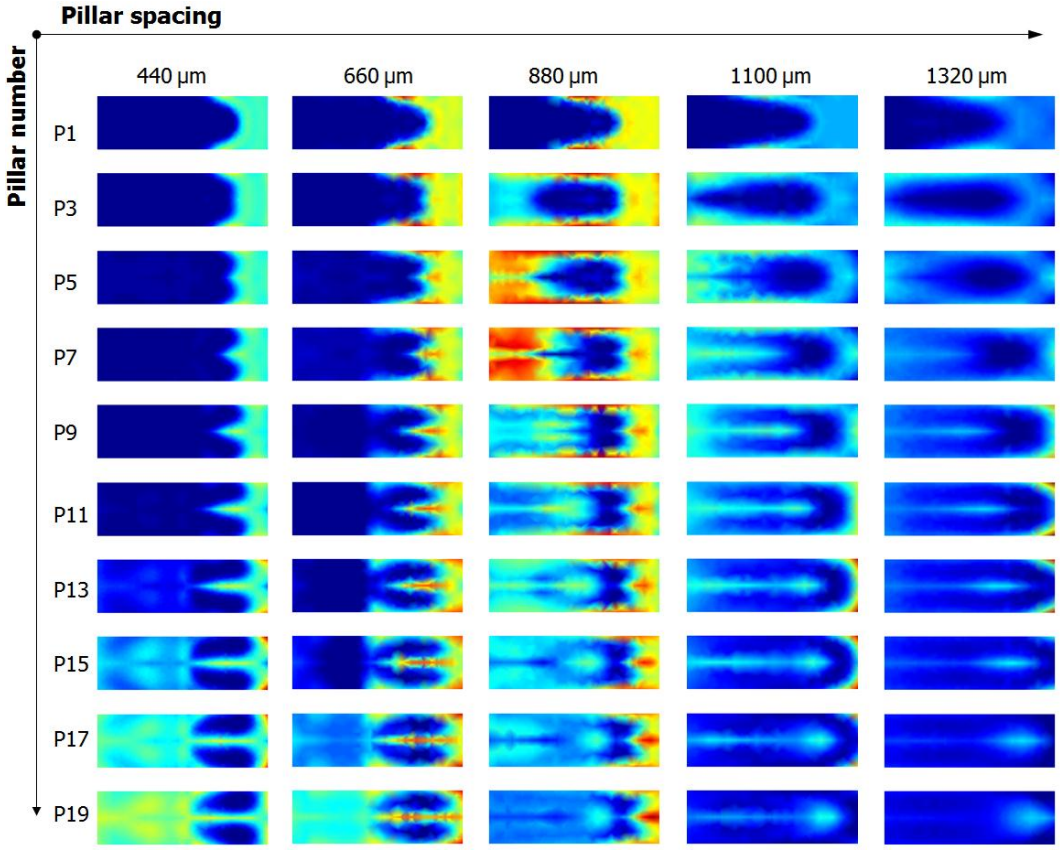

Figure S2. Evolution of secondary flow motion as a function of pillar number and spacing. For spacings shorter than 1.1 mm the secondary flows are less predictable because of non-linear superposition of the cross-sectional flow deformation caused by each pillar. Sequences with spacings above 1.1 mm behave as if deformations from single pillars were applied in series. All simulations were run at $Re = 100$.

Figure S3. Experimental confirmation of the secondary flow motion with a pillar spacing of 440 µm. **A**. (1) Fluorescent images from the top view as fluid flows downstream. (2) Corresponding numerical results. Vortices are formed after pillars and particles can become trapped there in some cases. Regardless of particle trapping in the vortices, pillar spacing below 1.1 mm showed lower focusing efficiency. Scale bar represents 200 µm. **B.** (1) Confocal fluorescent images show the folding of fluorescent dye solution injected with DI water as co-flow (operated at *Re* =100). (2) Confocal fluorescent images (false color) when dye is introduced in the other half of the channel. (3) FEM simulation results. Scale bar represents 100 µm.

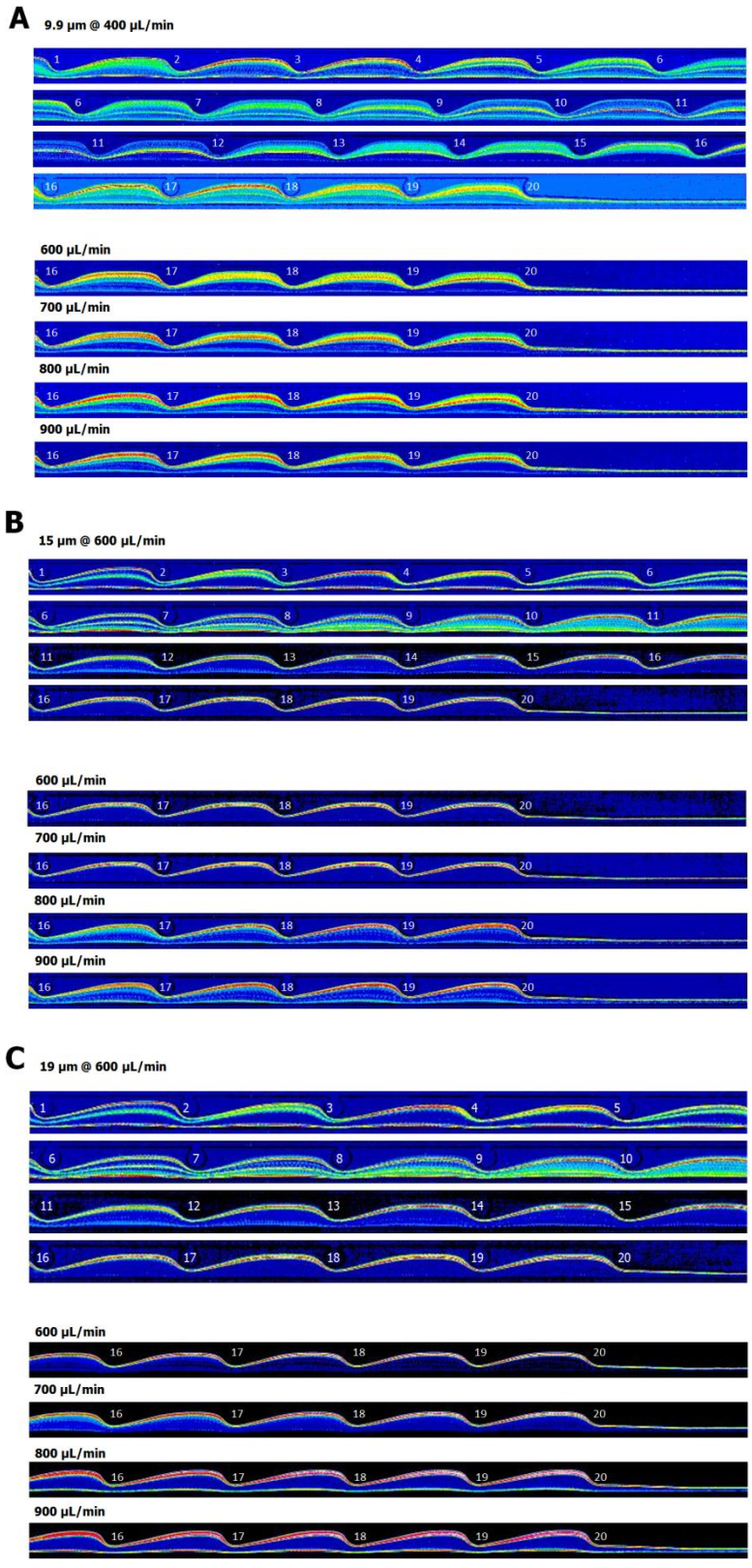

Figure S4. Standard deviation plots from high-speed image stacks (N = 4,000 images) describing qualitative lateral migration of particles at different flow rates for **A**. 9.9 µm polystyrene microspheres, **B.** 15 µm polystyrene microspheres, and **C.** 19 µm polystyrene microspheres.

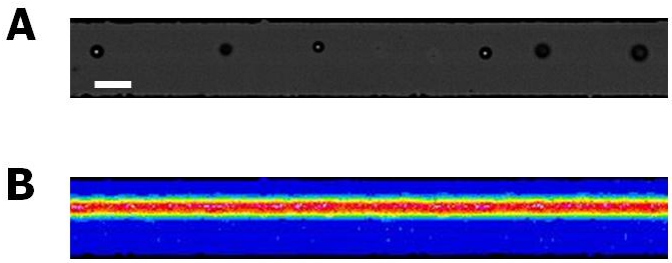

Figure S5. Two equilibrium positions. To confirm there are two particle equilibrium positions created by the combination of the secondary flows and channel shape, a 100 μm by 100 μm square channel is introduced instead of using the high aspect ratio channel (50 μm x 100 μm). **A.** A snapshot from a high-speed image stack that clearly shows two separate equilibrium positions. **B.** STD plots from same image stack. Scale bar represents 50 μm.

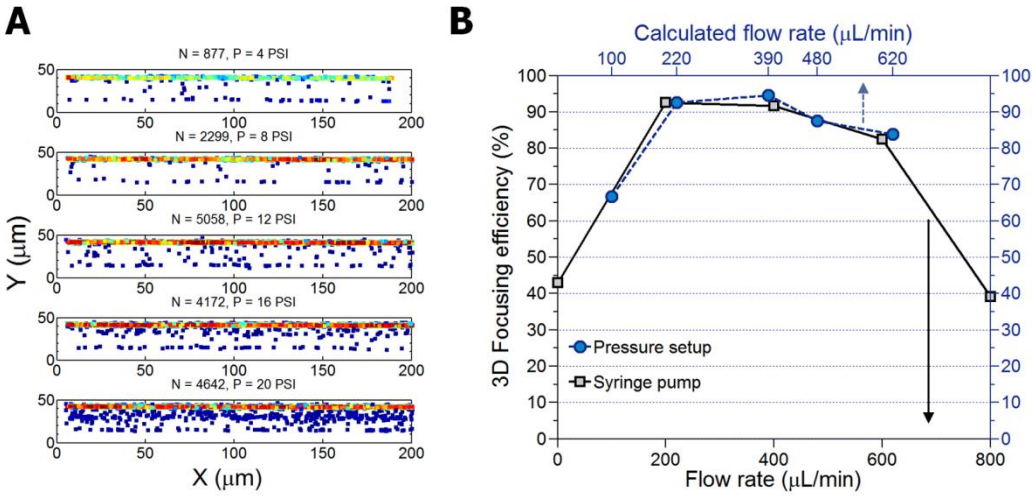

Figure S6. Focusing quality results using a pressure injection setup. **A**. Density scatter plots of 19 μm polystyrene microsphere centroid positions in the high-aspect ratio channel region. As pressure increases, microspheres assemble to a single-stream, and start defocusing beyond 16 PSI. **B.** 3D focusing efficiency comparison between syringe pump and pressure injection. The focusing efficiency is unaffected regardless of injection method.

Supporting Movie Captions

Supplemental Movie S1. **Single-stream focusing.** A real-time video of 19 μm polystyrene microparticles focusing as they travel downstream.

Supplemental Movie S2. **A demonstration of 19 μm polystyrene microsphere focusing.** High speed microscopic movie of polystyrene particles being inertially focused in a single focal plane as a single-stream train.

Supplemental Movie S3. **A demonstration of HeLa cell focusing.** High speed microscopic movie of HeLa cells being inertially focused in a single focal plane as a single-stream train. Note that the image plane is intentionally out of focus to better distinguish the cell planes.

References

1. H. Amini, E. Sollier, W. M. Weaver and D. Di Carlo, *Proc. Natl. Acad. Sci. U.S.A*, 2012, **109**, 11593-11598.
2. A. J. Chung, D. R. Gossett and D. Di Carlo, *Small*, 2013, **9**, 685-690.